



# DFT studies of *N*-alkoxyaminy radicals: ESR parameters, UV–vis absorptions and generations

Akio Tanaka<sup>a,\*</sup>, Kouichi Nakashima<sup>a,†</sup>, Yoza Miura<sup>b</sup>

<sup>a</sup>Organic Synthesis Research Laboratory, Sumitomo Chemical Co., Ltd., 1-98, Kasugade-naka 3-chome, Konohana-ku, Osaka 554-8558, Japan

<sup>b</sup>Department of Applied Chemistry, Graduate School of Engineering, Osaka City University, Sumiyoshi-ku, Osaka 558-8585, Japan

## ARTICLE INFO

### Article history:

Received 3 November 2010

Received in revised form 23 January 2011

Accepted 25 January 2011

Available online 2 February 2011

### Keywords:

*N*-Alkoxyaminy radical

Aminoxy radical

ESR

Hyperfine coupling constant

*g*-Factor

TD-DFT

UV–vis

DFT

IEFPCM

Coupled cluster

Reaction mechanism

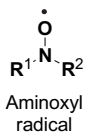
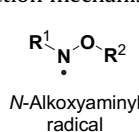
## ABSTRACT

Although aminoxy radicals (RR'N $\dot{O}$ ) are well-known as organic stable free radicals, the isomeric radicals, *N*-alkoxyaminy radicals (RNOR'), are scarcely studied in the area of theoretical study. We carried out the theoretical calculation of the isotropic <sup>14</sup>N hyperfine coupling constants (*a*<sub>N</sub>), *g*-factors, electronic absorbances, and generation mechanisms of *N*-alkoxyaminy radicals. For thirty one *N*-alkoxyaminy radicals, the PCM-DFT calculation at B3LYP/6-31+G(d,p) could well reproduce the experimental data of *a*<sub>N</sub> and *g*-factors, where *R*<sup>2</sup> were 0.9796 and 0.9439, respectively. The UV–vis spectra were moderately reproduced by PCM-TD-DFT (PBE0/6-31+G(d,p)), where *R*<sup>2</sup> was 0.9205. Additionally, the use of a linear scaling procedure precisely reproduced the UV–vis spectrum. The activation Gibbs free energies for the generation of *N*-alkoxyaminy radicals and aminoxy radicals in the competing reactions of nitroso compounds with alkyl radicals were estimated by DFT and coupled cluster calculations. The activation free energies for the generation of *N*-alkoxyaminy radicals were estimated to be 9–18 kcal/mol at B3LYP/6-31+G(d,p). The reported product ratios in the competing reactions could be reasonably explained by the differences in the activation free energies.

© 2011 Elsevier Ltd. All rights reserved.

## 1. Introduction

Stable organic free radicals are still rare because of their high reactivities derived from the open shell orbital.<sup>1</sup> The magnetic properties of stable radicals have been applied to the structure elucidation of biochemical compounds<sup>2</sup> and to the study of organic magnetic<sup>3</sup> and conductive materials.<sup>4</sup> The reactivities have provided several oxidants for alcohol or aldehyde compounds<sup>5</sup> and mediators for controlled free radical polymerization.<sup>6</sup> In addition, relatively long-lifetime radicals generated in homolytic reactions have sometimes been characterized by ESR measurement to understand the reaction mechanism.<sup>7</sup>



Among the reported stable radicals, a variety of hetero atom-centered free radicals have been included. Aminoxy radicals are one of the most well-known hetero atom-centered free radicals and have been widely studied over a long time due to the easiness of syntheses and their stabilities.<sup>1</sup> The first isolation of monomeric organic aminoxy radical has been reported by Piloty and Schwerin in 1901.<sup>8</sup> In contrast, *N*-alkoxyaminy radicals have been later discovered and the study of the radicals are still limited, though *N*-alkoxyaminy radicals have the same components as aminoxy radicals. In 1967, the existence of *N*-alkoxyaminy radical was first reported by Balaban,<sup>9</sup> and in 1971 two groups reported the different synthetic methods to determine the hyperfine coupling constants (hfccs) and *g*-factors by ESR. One group generated *N*-alkoxyaminy radicals by the reactions of substituted nitrosobenzenes with carbon-centered radicals,<sup>10</sup> and the other generated photodecomposition of *tert*-butyl peroxy carbamates.<sup>11</sup> In 2001, Miura succeeded in the first isolation of *N*-alkoxyaminy radicals as single crystals<sup>12</sup> and determined their X-ray crystal structures and magnetic properties.<sup>13</sup> With regard to their theoretical calculations, Miura has performed the DFT calculations to estimate the spin density distributions using the crystal geometries.<sup>12,13</sup> However, no detailed theoretical calculations for the radicals have been investigated.<sup>14</sup> In this paper, we wish to report the theoretical study of ESR parameters, electronic

\* Corresponding author. E-mail address: [tanakaa1@sc.sumitomo-chem.co.jp](mailto:tanakaa1@sc.sumitomo-chem.co.jp) (A. Tanaka).

† Present address: Material Science and Technology, Interdisciplinary Graduate School of Medical and Engineering, University of Yamanashi, Kofu, Yamanashi 400-8510, Japan.

absorption, and generation mechanism of *N*-alkoxyaminyl radicals, using DFT, TD-DFT, and coupled cluster calculations.

## 2. Computational details

Three hybrid exchange–correlation DFT calculations were performed for the purpose of optimization of geometries, predictions of excited states, and analyses of vibrational frequencies with 6-31+G(d,p)<sup>15</sup> basis set using the Gaussian03 package.<sup>16</sup> Natural atomic charges and spin densities for radicals were obtained by natural population analyses (NPA) using the NBO program version 3.1.<sup>16b</sup> Two hybrid functionals are linear combinations of Hartree-Fock, LDA and B88, so-called three-parameter hybrid (B3LYP),<sup>17</sup> and the Becke-Half-and-Half-LYP (BHandHLYP)<sup>18</sup> introduced by Becke. Third one is PBE0 developed by Adamo and Barone based on the PBE GGA by Perdew, Burke, and Ernzerhof.<sup>19</sup> The B3LYP, PBE0, and BHandHLYP include 20%, 25%, and 50% exact HF exchange energies, respectively. Calculations of <sup>14</sup>N hfccs ( $a_N$ ) and  $g$ -factor were carried out with B3LYP and BHandHLYP functionals. The BHandHLYP has been reported to predict accurately ESR parameters for aminoxyl radicals.<sup>20</sup> The time-dependent DFT calculation (TD-DFT)<sup>21</sup> were performed by B3LYP and PBE0 functionals, which have been recommended in previous studies for other radicals.<sup>3b,22</sup> In addition, a solvation method of the polarizable continuum model (PCM) using the integral equation formalism variant (IEF)<sup>23</sup> were considered in the TD-DFT calculations, where the geometries were optimized by the same calculation levels including solvent effects. The same solvents as the experimental data were specified in the IEFPCM calculations to predict the ESR parameters (Table 2) and UV–vis spectra (Table 4). To estimate reactivity and selectivity of radicals, activation energies were calculated by B3LYP at the gas phase. For some small molecules, the coupled cluster method CCSD(T)<sup>24</sup> were also carried out using the geometries and corrections of enthalpy and Gibbs free energies obtained from the result of vibrational frequency analyses at the B3LYP level. All geometries of ground and transition states in Figs. 9–11 are available in the Supplementary data.

## 3. Results and discussion

### 3.1. Isotropic $a_N$ and $g$ -factor of *N*-alkoxyaminyl radicals

The density functional theory has been known to demonstration for good performance to predict NMR and ESR parameters as examined in several reviews.<sup>25</sup> Although there are some previous papers to study DFT calculations of isotropic hfccs and  $g$ -factors for nitrogen-centered organic radicals,<sup>26</sup> *N*-alkoxyaminyl radicals has not been discussed in detail. In this section, two hybrid functionals, B3LYP, and BHandHLYP, have been performed for 31 reported *N*-alkoxyaminyl radicals to study reproducibility of  $a_N$  and  $g$ -factors. Before the systematic calculations, *N*-methoxymethylaminyl radical (MeNOMe) and *N,N*-dimethylaminoxyl radical (Me<sub>2</sub>NÖ), the simplest structure of *N*-alkoxyaminyl and aminoxyl radicals, have been first calculated for comparison of Gibbs free energies, N–O bond distances and natural spin densities, natural charges, and  $a_N$  and  $g$ -factors at the B3LYP/6-311++G(2df,2dp) (Table 1).

**Table 1**

Optimized N–O bond distances, spin densities, charges, isotropic  $a_N$  and  $g$ -factors of MeNOMe and Me<sub>2</sub>NÖ at B3LYP/6-311++G(2df,2dp) in benzene using IEFPCM model

Radical	Relative Gibbs free energy (kcal/mol)	N–O Distance(Å)	Spin density <sup>a</sup>		Charge <sup>b</sup>		$a_N$ <sup>c</sup> (mT)	$g$ -factor <sup>d</sup>
			N	O	N	O		
MeNOMe	+13.1	1.364	0.786	0.170	–0.094	–0.401	1.162	2.00498
Me <sub>2</sub> NÖ	0.0	1.277	0.469	0.498	0.004	–0.444	0.889	2.00611

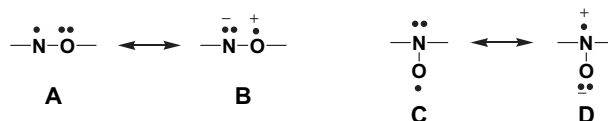
<sup>a</sup> Natural spin density.

<sup>b</sup> Natural atomic charge.

<sup>c</sup> Isotropic  $a_N$ .

<sup>d</sup> Isotropic  $g$ -factor.

In comparison with Me<sub>2</sub>NÖ, MeNOMe is thermodynamically less stable by 13.1 kcal/mol, the N–O bond distance is longer, and the spin density on nitrogen is much higher than that of Me<sub>2</sub>NÖ. This can be explained in terms that the contribution of the dipolar canonical structure **B** to the resonance hybrid of Me<sub>2</sub>NÖMe is less effective than that of the dipolar canonical structure **D** to the hybrid of Me<sub>2</sub>NÖ because the electronegativity of nitrogen is less than oxygen.<sup>27</sup> The spin density distributions of the two radicals reflect to the difference in their  $g$ -factors, where the  $g$ -factor of MeNOMe and Me<sub>2</sub>NÖ are 2.00498 and 2.00611, respectively.



Next, using the experimental  $a_N$  and  $g$ -factors for 31 *N*-alkoxyaminyl radicals, reproducibility of DFT calculations has been evaluated including IEFPCM solvation model. The radicals consist of the isolated radicals, **1–12**, *tert*-butyl-substituted radicals **13–18**, electron-withdrawing and -donating group substituted-radicals **19–24**, *N*-alkoxycarbonyl substituted-radicals **25** and **26**, and *N*-alkoxyalkylaminyl radicals **27–31** (Fig. 1).

Table 2 summarizes the theoretical and experimental  $a_N$  and  $g$ -factors for **1–31**. Table 3 lists the intercept and slope of correlation equations, and the mean absolute errors (MAE) between the theoretical and experimental data.

From  $R^2$  shown in Table 3, B3LYP functional gives better agreement with the experimental data than BHandHLYP. The isotropic  $a_N$  calculated by B3LYP are in good agreement with the experimental data as shown in Fig. 2, where  $R^2$  is 0.9796 and MAE is 0.035 mT. Although, the  $a_N$  estimated by BHandHLYP are linearly correlated with the experimental, the functional overestimates them by about 0.5 mT. The estimation errors by BHandHLYP for *N*-alkoxyaminyl radicals have not been reported in the estimation for aminoxyl radicals.<sup>20</sup> Hfccc are generally dependent on the spin densities on nitrogens. At B3LYP, the spin densities on nitrogen of **1–10** and **13–24** range from 0.503 to 0.583, and those of **25** and **26** are 0.618 and 0.607, respectively. On the other hand, those of **11** and **12** are 0.402 and 0.396, which are much lower than those of **1–10** and **13–26**. This indicates a larger delocalization of the unpaired electron spin onto the pyrene ring in **11** and **12**. In contrast, those of **27–31** showed relatively larger  $a_N$  with around 0.79 because of negligibly-small ability to delocalize the unpaired electron spin over alkyl groups. The calculated  $g$ -factors are also in good agreement with the experimental data (Fig. 3), where  $R^2$  is 0.9439, and MAE is 0.0001 at B3LYP. On the basis of the above results, it can be confirmed that  $a_N$  and  $g$ -factors of *N*-alkoxyaminyl radicals are well reproduced by IEFPCM/B3LYP/6-31+G(d,p).

### 3.2. Electronic absorption spectroscopy of *N*-alkylarylaminy radical

Theoretical studies of electronic absorptions for organic compounds are still one of the important problems in organic and

**Table 2**  
Experimental and theoretical isotropic  $a_N$  and  $g$ -factors of  $N$ -alkoxyaminy radicals

Radical	Experimental <sup>a</sup>			IEFPCM/B3LYP/6-31+G(d,p) <sup>b</sup>			IEFPCM/BHandHLYP/6-31+G(d,p) <sup>b</sup>		
	$a_N$ (mT)	$g$ -factor	Ref	$a_N$ (mT) <sup>c</sup>	$g$ -factor <sup>d</sup>	Spin density <sup>e</sup>	$a_N$ (mT) <sup>c</sup>	$g$ -factor <sup>d</sup>	Spin density <sup>e</sup>
1	1.01	2.0042	12a	1.054	2.00421	0.537	1.550	2.00443	0.631
2	0.997	2.0041	12a	1.042	2.00424	0.533	1.581	2.00437	0.636
3	0.999	2.0042	12a	1.038	2.00432	0.532	1.579	2.00445	0.636
4	0.987	2.0038	12a	1.052	2.00393	0.539	1.605	2.00406	0.644
5	1.05	2.0043	12b	1.043	2.00429	0.541	1.578	2.00439	0.638
6	1.00	2.0041	12b	1.005	2.00420	0.523	1.542	2.00431	0.625
7	0.984	2.0043	12b	0.996	2.00438	0.519	1.531	2.00450	0.622
8	1.016	2.0042	13b	1.020	2.00426	0.531	1.558	2.00437	0.634
9	0.993	2.0039	13c	1.040	2.00405	0.535	1.590	2.00417	0.639
10	0.965	2.0040	13c	1.026	2.00404	0.526	1.576	2.00416	0.633
11	0.672	2.0035	13a	0.789	2.00378	0.402	1.295	2.00391	0.512
12	0.675	2.0037	13a	0.780	2.00375	0.396	1.289	2.00389	0.508
13	1.026	2.0040	28	1.037	2.00402	0.514	1.566	2.00412	0.614
14	1.001	2.0037	28	1.017	2.00374	0.503	1.549	2.00385	0.601
15	1.033	2.0040	28	1.046	2.00411	0.523	1.578	2.00419	0.620
16	1.053	2.0036	28	1.056	2.00369	0.544	1.602	2.00385	0.645
17	1.07	2.0043	29	1.141	2.00425	0.583	1.681	2.00432	0.665
18	1.05	2.0040	29	1.112	2.00419	0.571	1.642	2.00425	0.658
19	1.095	2.0044	30	1.131	2.00426	0.583	1.667	2.00431	0.667
20	1.062	2.0046	30	1.113	2.00481	0.573	1.650	2.00482	0.660
21	0.995	2.0046	30	1.011	2.00480	0.530	1.558	2.00485	0.637
22	1.074	2.0046	30	1.128	2.00420	0.578	1.669	2.00427	0.664
23	1.073	2.0042	30	1.124	2.00430	0.570	1.685	2.00437	0.662
24	1.01	2.0046	30	1.047	2.00471	0.544	1.588	2.00484	0.643
25	1.08	2.0056	30	1.100	2.00567	0.618	1.541	2.00566	0.681
26	1.08	2.0057	30	1.100	2.00576	0.607	1.543	2.00576	0.671
27	1.447	2.0048	30	1.468	2.00483	0.788	2.003	2.00485	0.837
28	1.428	2.0048	30	1.442	2.00479	0.790	1.966	2.00482	0.839
29	1.43	2.0048	30	1.449	2.00479	0.792	1.976	2.00480	0.841
30	1.431	2.0048	30	1.425	2.00474	0.794	1.943	2.00477	0.843
31	1.41	2.0049	27	1.408	2.00481	0.792	1.929	2.00483	0.841

<sup>a</sup> Compound **11** and **12** in toluene, and others in benzene.

<sup>b</sup> The same solvents as the experimental ones were used in the calculations.

<sup>c</sup> Isotropic  $a_N$ .

<sup>d</sup> Isotropic  $g$ -factor.

<sup>e</sup> Natural spin density via NPA.

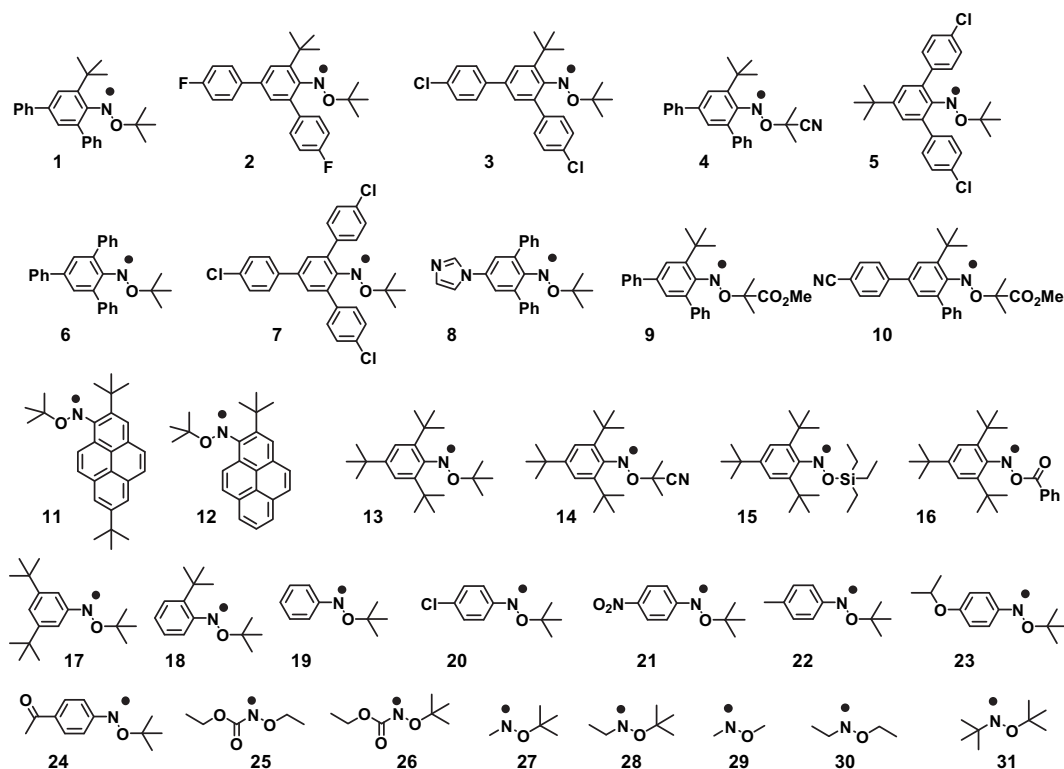


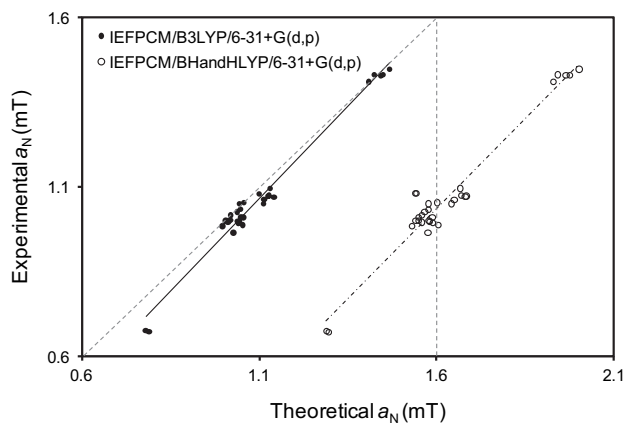
Fig. 1.  $N$ -alkoxyaminy radicals.

**Table 3**  
Correlation analyses between the experimental and predicted  $a_N$  and  $g$ -factors

	IEFPCM/B3LYP/6-31+G(d,p)		IEFPCM/BHandHLYP/6-31+G(d,p)	
	$a_N$	$g$ -factor	$a_N$	$g$ -factor
$R^2$	0.9796	0.9439	0.9737	0.9294
Intercept	-0.1309	-0.0317	-0.6615	-0.1935
Slope	1.0879	1.0158	1.061	1.0965
MAE <sup>a</sup>	0.0347	0.0001	0.5616	0.0002

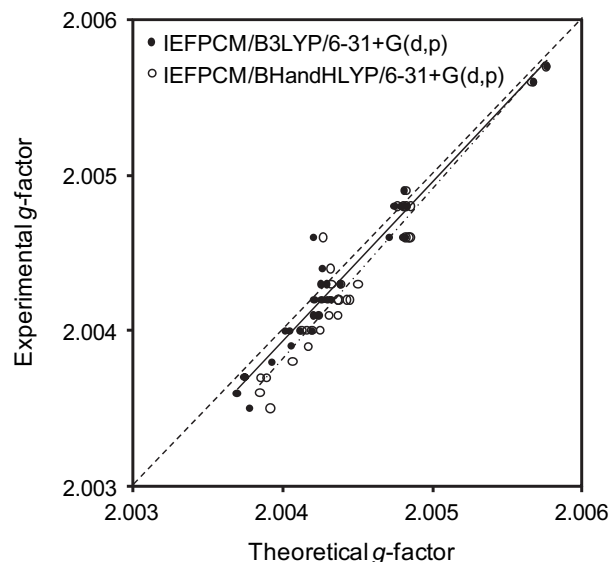
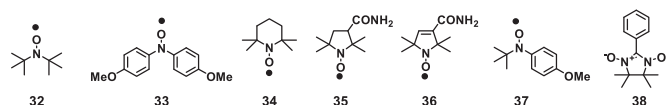
<sup>a</sup> Mean absolute error.**Table 4**  
Experimental and theoretical longest wavelengths (nm) and excitation energies (eV)

Radical	Experimental <sup>a</sup>			IEFPCM/B3LYP/6-31+G(d,p) <sup>b</sup>		IEFPCM/PBE0/6-31+G(d,p) <sup>b</sup>		
	Solvent	nm	eV	Ref	nm	eV	nm	eV
<b>1</b>	Benzene	545	2.275	12a	508.8	2.437	487.8	2.542
<b>2</b>	Benzene	545	2.275	12a	507.7	2.442	495.0	2.505
<b>3</b>	Benzene	533	2.326	12a	508.1	2.441	496.2	2.499
<b>5</b>	Benzene	492	2.520	12b	477.9	2.595	461.1	2.689
<b>6</b>	Benzene	542	2.288	12b	490.5	2.528	473.1	2.621
<b>7</b>	Benzene	546	2.271	12b	496.5	2.497	478.1	2.593
<b>8</b>	Benzene	514	2.412	13b	493.8	2.511	476.2	2.604
<b>9</b>	Benzene	541	2.292	13c	501.0	2.475	487.9	2.541
<b>10</b>	Benzene	539	2.301	13c	531.1	2.335	506.2	2.449
<b>32</b>	Acetonitrile	453	2.737	32	447.2	2.773	430.9	2.878
<b>33</b>	Acetonitrile	502	2.470	32	494.7	2.506	475.0	2.611
<b>34</b>	Acetonitrile	463	2.678	32	459.2	2.701	441.8	2.807
<b>35</b>	Acetonitrile	428	2.897	32	416.2	2.979	401.3	3.089
<b>36</b>	Acetonitrile	438	2.831	32	415.6	2.984	400.5	3.095
<b>37</b>	Acetonitrile	490	2.531	32	468.1	2.649	450.5	2.752
<b>38</b>	Acetonitrile	583	2.127	32	548.2	2.262	516.2	2.402

<sup>a</sup> Lowest energy absorption.<sup>b</sup> The same solvents as the experimental ones were used in the calculations.**Fig. 2.** Plots of theoretical versus experimental  $a_N$  for  $N$ -alkoxyaminyls. The data-points ● and the solid line indicates the theoretical  $a_N$  by IEFPCM/B3LYP/6-31+G(d,p), the points ○ and the dash-dotted line indicate  $a_N$  estimated by and IEFPCM/BHandHLYP/6-31+G(d,p), respectively.

theoretical chemistry. TD-DFT is one of the most successful theories to estimate the properties from the viewpoint the accuracy and computational cost.<sup>31</sup> To investigate excitation energies for  $N$ -alkoxyaminyl radicals, TD-DFT calculations have been carried out. The UV–vis spectra of the nine radicals **1**, **2**, **3**, **5**, **6**, **7**, **8**, **9**, and **10** have been reported, but the range of the longest absorption wavelengths in their UV–vis spectra is narrow, 500–550 nm, due to the similar structures each other. For the purpose of understanding the wider range of electronic absorptions, we furthermore calculated the spectra for seven aminoxy radicals **32–38** (Fig. 4).

As for the experimental UV–vis spectra, the nine  $N$ -alkoxyaminyl radicals have been measured in benzene<sup>12,13</sup> and the seven

**Fig. 3.** Plots of theoretical versus experimental  $g$ -factors for  $N$ -alkoxyaminyls. The data-points ● and the solid line indicates the theoretical  $g$ -factors by IEFPCM/B3LYP/6-31+G(d,p), the points ○ and the dash-dotted line indicate the  $g$ -factors estimated by IEFPCM/BHandHLYP/6-31+G(d,p), respectively.**Fig. 4.** Aminoxy radicals.

aminoxy radicals have been done in acetonitrile.<sup>32</sup> Since the spectra are influenced by solvent properties, the solvent effects have been taken into account in the theoretical calculations.<sup>33</sup> Both geometry optimization and TD-DFT calculations were carried out at B3LYP and PBE0 functionals with IEFPCM solvation model (Table 4).

From the results of IEFPCM-TD-DFT calculations, PBE0 functional was found to be in better agreement with the experimental data than B3LYP, where  $R^2$  from B3LYP/6-31+G(d,p) and PBE0/6-31+G(d,p) were 0.9136 and 0.9205 at eV, respectively (Table 5). Fig. 5 describes the correlation plots between the longest experimental and theoretical wavelength calculated by IEFPCM/PBE0/6-31+G(d,p). It shows the theoretical wavelengths are 0.35 eV shorter than the experimental.

**Table 5**  
Correlation analysis of experimental and theoretical longest wavelengths (nm) and excitation energies (eV)

	IEFPCM/B3LYP/6-31+G(d,p)		IEFPCM/PBE0/6-31+G(d,p)	
	nm	eV	nm	eV
$R^2$	0.8985	0.9136	0.9058	0.9205
Intercept	-55.1	0.284	-74.3	-0.345
Slope	1.164	1.605	1.2450	1.049
MAE <sup>a</sup>	24.3	0.118	42.3	0.215

<sup>a</sup> Mean absolute error.

To investigate the molecular orbitals causing electronic absorptions, the UV–vis spectrum of **1** (Fig. 6)<sup>12b</sup> was reproduced using the 11 longest wavelengths provided by the TD-DFT calculation at IEFPCM/PBE0/6-31+G(d,p). In the spectrum, the origins of the absorptions at longer and weaker absorption area have been elaborated.

The experimental spectrum of **1** indicates a strong absorption at 334 nm and a weak absorption at 545 nm. Additionally, there is a different weak absorption at around 440 nm. While the measured

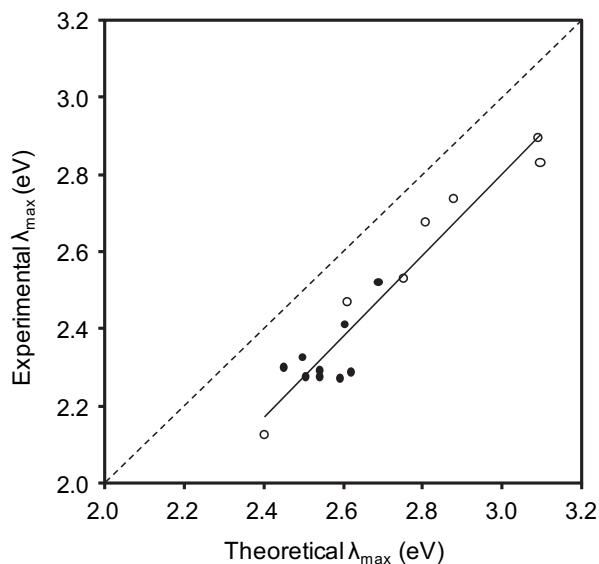


**Fig. 5.** Plots of the experimental and theoretical longest wavelengths of radicals. The TD-DFT calculations were performed by IEFPCM/PBE0/6-31+G(d,p). The data-points ● and ○ indicate *N*-alkoxyaminy and aminoxy radicals, respectively.

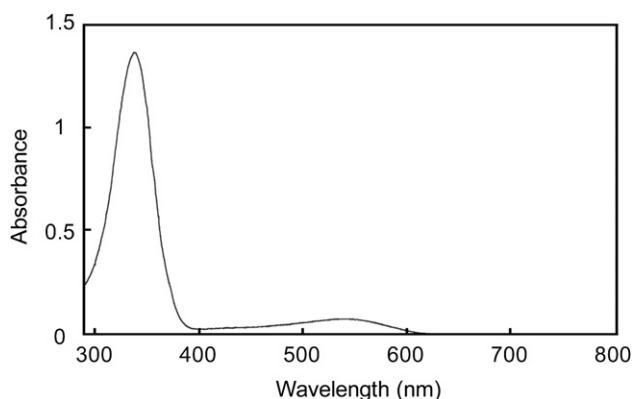


**Fig. 6.** UV-vis spectrum of **1** in benzene solution.

longest wavelength was 545 nm, the longest theoretical was 488 nm (Table 4). To correct the gap between the theoretical and experimental data, the theoretical excitation energies in eV were linearly scaled using the correlation equation.<sup>22b</sup> The equation is  $\text{Exp. (eV)} = 1.049 \text{ calcd (eV)} - 0.345$ , which has been derived from the longest wavelengths between the calculated and experimental data (Table 5). From the linearly scaled excitation energies, the UV-vis spectrum was reproduced by conversion to the gaussian function curve composing of the full width at half-maximum set by 0.4 eV and the absorptivity using the oscillator strength for each absorption.<sup>34</sup> The generated spectrum converted in nm is shown in Fig. 7.

Table 6 summarizes excitation energies, linearly scaled excitation energies, wavelengths, oscillator strengths, and excited molecular orbitals of the main three absorptions for **1** estimated by IEFPCM-TD-DFT at PBE0/6-31+G(d,p). The shapes of eight related frontier orbitals are shown in Fig. 8, and the corresponding energy levels of  $\alpha$  and  $\beta$  spins are described in the Supplementary data.

The simulated UV-vis spectrum (Fig. 7) reproduces excellently the experimental one (Fig. 6). The observed absorptions at 545 and 440 nm correspond to the theoretical absorptions at 534 and 460 nm that have been scaled from 488 to 428 nm. The longest wavelength absorption is mainly derived from  $n \rightarrow \pi^*$  transition ( $\beta\text{HOMO} \rightarrow \beta\text{LUMO}$ , which denotes transition of  $\beta$  spin from HOMO to LUMO). The  $\beta\text{HOMO}$  orbital spreads over  $\dot{\text{N}}\text{O}$  radical center and

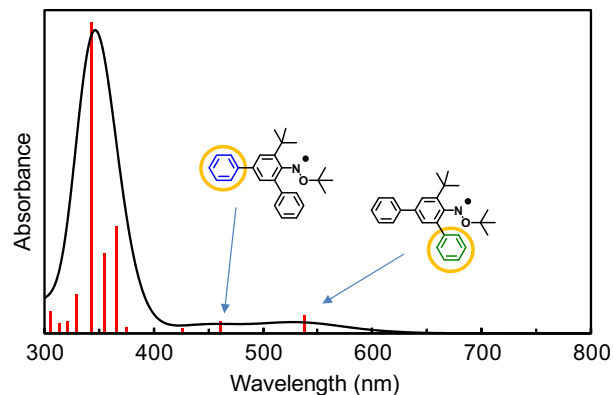


**Fig. 7.** UV-vis spectrum of **1** in benzene solution simulated by IEFPCM-TD-DFT at PBE0/6-31+G(d,p) level including linear scale procedure.

**Table 6**

Theoretical vertical excitation energy, wavelength, oscillator strength, and fraction composition of **1** calculated at IEFPCM/PBE0/6-31+G(d,p)

States	Excitation energy(eV)	Wavelength (nm)	Oscillator strength	Composition <sup>a</sup>
1 <sup>2</sup> A	2.542	487.8	0.0222	$\beta\text{H}-0 \rightarrow \beta\text{L}+0$ (51%)
	(2.321) <sup>b</sup>	(534.2)		$\beta\text{H}-5 \rightarrow \beta\text{L}+0$ (20%)
				$\beta\text{H}-2 \rightarrow \beta\text{L}+0$ (16%)
2 <sup>2</sup> A	2.898	427.9	0.0145	$\beta\text{H}-1 \rightarrow \beta\text{L}+0$ (28%)
	(2.695)	(460.2)		$\alpha\text{H}-0 \rightarrow \alpha\text{L}+0$ (21%)
				$\beta\text{H}-5 \rightarrow \beta\text{L}+0$ (11%)
7 <sup>2</sup> A	3.767	329.1	0.4566	$\alpha\text{H}-0 \rightarrow \alpha\text{L}+0$ (25%)
	(3.607)	(343.8)		$\beta\text{H}-1 \rightarrow \beta\text{L}+0$ (13%)
				$\beta\text{H}-0 \rightarrow \beta\text{L}+1$ (11%)

<sup>a</sup>  $\alpha, \alpha$  spin orbital;  $\beta, \alpha$  spin orbital; H, HOMO (highest occupied molecular orbital); L, LUMO (lowest unoccupied molecular orbital).

<sup>b</sup> In parentheses, scaled values are equal to  $1.049 \text{ calcd} - 0.345$  (eV).

the 2-phenyl group. The next longest wavelength around 440 nm, originates from  $\pi \rightarrow \pi^*$  transition ( $\beta\text{HOMO}-1 \rightarrow \beta\text{LUMO}$ ). The  $\beta\text{HOMO}-1$  orbital is over the  $\dot{\text{N}}\text{O}$  and 4-phenyl group. In other words, the two weak absorptions of the longest and the next longest wavelengths of **1** are attributed to the orbitals of the radical center and the two substituted phenyl rings substituted at 2 and 4 positions (Fig. 7).

### 3.3. Generation of *N*-alkoxyaminy radicals

Among the reported synthetic methods of *N*-alkoxyaminy radicals, the most widely used method is the reaction of nitroso compounds with alkyl radicals generated in situ from appropriate sources. As for the generation, for example, photolysis of diazo compounds, the reaction of alkyl halides with trialkyl-stannanes, and the reaction of active methylene with benzoyl peroxide have been used.<sup>13c,28</sup> The addition of alkyl radicals to nitroso compounds often causes a couple of competing reactions: one is the radical attack to the nitroso nitrogen, which yields aminoxy radicals, and the other is the radical attack to the nitroso oxygen yielding *N*-alkoxyaminy radicals. The *N*-alkoxyaminy/aminoxy ratio depends on both the steric congestions around the nitroso group and the bulkiness of attacking alkyl radicals.

In this section, the reactions of nitroso compounds with alkyl radicals have been theoretically investigated. The results are summarized in Table 7. **S1** is the reaction of 1,1-dimethylnitrosoethane (<sup>t</sup>BuNO) with <sup>t</sup>Bu radical (CMe<sub>3</sub>).<sup>27</sup> **S2** is the reaction that has reported to generate *N*-alkoxyaminy exclusively.<sup>35</sup> **S3** to **S7** are the reactions of nitrosobenzene and its derivatives with carbon radicals. The reaction of nitrosobenzene with methyl radical (**S3**) has been demonstrated as a model reaction. The reactions of **S4–S7**



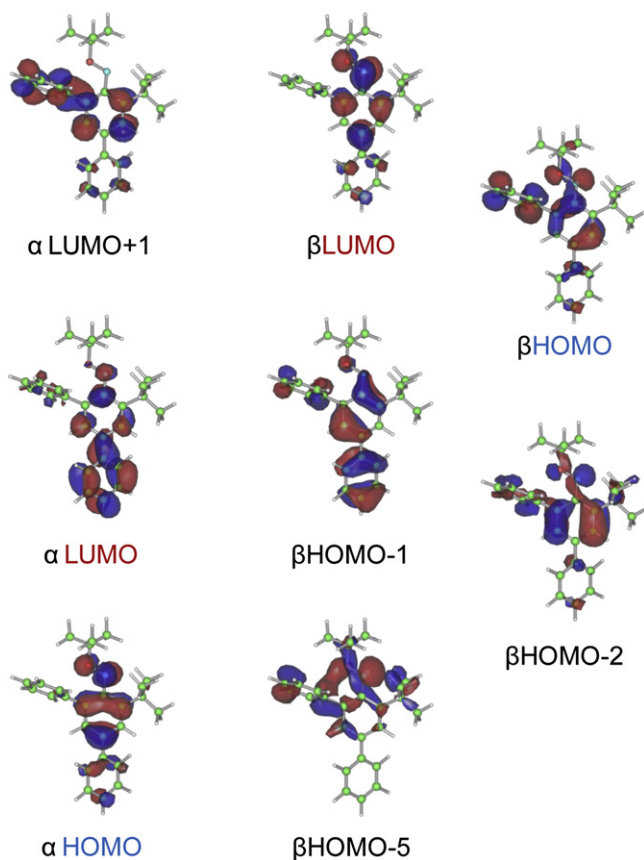


Fig. 8. Frontier orbitals of **1**.

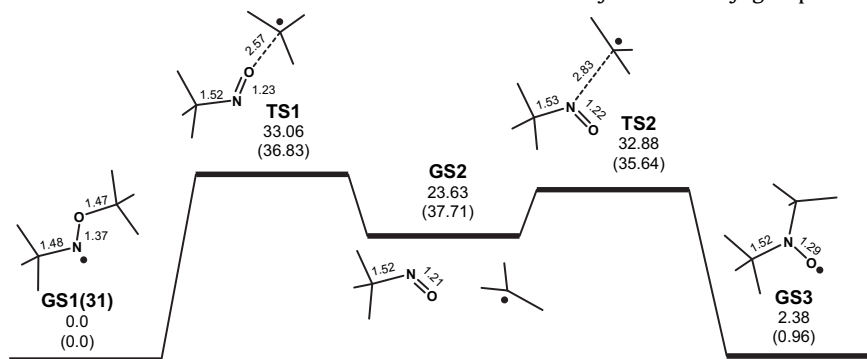


Fig. 9. The relative Gibbs free-energy diagram of rearrangement of **31** to  ${}^t\text{Bu}_2\text{NO}$  at CCSD(T)/6-31+G(d,p)//B3LYP/6-31+G(d,p), and the numbers in parentheses indicate enthalpies based on GS1 in kcal/mol. The numbers around bonds in each structure indicates the bond distances in angstrom.

have already been reported<sup>12a,13c,28</sup> and the *N*-alkoxyaminy/aminoxyl ratios are described in the corresponding papers. In **S4**, aminoxyl radical alone was observed as the adduct, and in **S5** and **S6** both *N*-alkoxyaminy and aminoxyl radicals were observed. In

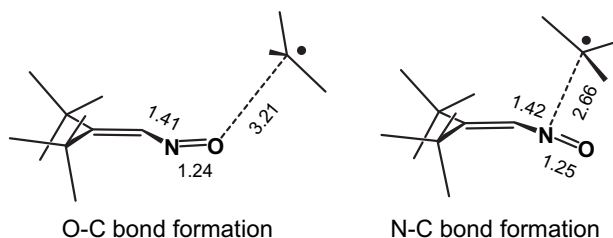


Fig. 10. Transition state structures for O–C and N–C bond formation in **S2**. The numbers in each transition states are the bond distances in angstrom.

**S7**, on the other hand, *N*-alkoxyaminy alone was observed. In the present study, the activation energies and heat of reactions for **S1–S7** have been calculated at B3LYP/6-31+G(d,p). In addition, CCSD(T)/6-31+G(d,p)//B3LYP/6-31+G(d,p) levels for **S1** and **S3** have been executed to obtain the insight into the selectivity in the radical addition reactions.

The theoretical activation Gibbs free energy for the generation of  ${}^t\text{BuNO}{}^t\text{Bu}$  (**31**) is 11.52 kcal/mol and that for  ${}^t\text{Bu}_2\text{NO}$  is 12.72 kcal/mol at B3LYP/6-31+G(d,p), which means that the generation of **31** is predominant over  ${}^t\text{Bu}_2\text{NO}$ . On the other hand, the activation energies estimated by CCSD(T)/6-31+G(d,p) show almost the same between the competing reactions (Table 7).

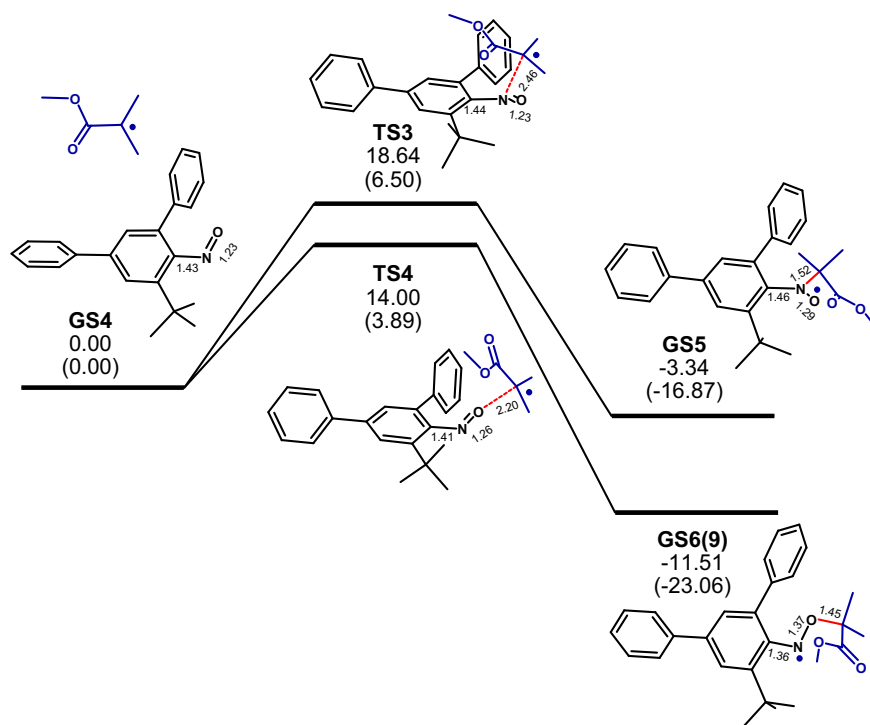
Ingold reported that **31** did not undergo the intramolecular radical rearrangement to  ${}^t\text{Bu}_2\text{NO}$  because the  $\text{sp}^3$  orbital of carbon has no orbital to accept the unpaired electron at the transition state, unlike with the reported rearrangement of  $\text{Me}_3\text{SiNOSiMe}_3$  to  $(\text{Me}_3\text{Si})_2\text{NO}$ .<sup>27</sup> The rearrangement of **31** to  ${}^t\text{Bu}_2\text{NO}$  might be possible only when the O–C cleavage in **31** takes place to generate  ${}^t\text{BuNO}$  and  $\dot{\text{C}}\text{Me}_3$  followed by recombination to yield  ${}^t\text{Bu}_2\text{NO}$ . From the measurement of the radical persistent, Ingold has estimated the activation energy for O–C bond cleavage to be  $\geq 28$  kcal/mol. From the activation energies and heat of reactions of **S1**, we built a relative free-energy diagram for  $\beta$ -scission and recombination of **31** as shown in Fig. 9.

The theoretical activation free energy for the  $\beta$ -scission corresponding to the step GS1(**31**) to TS1 is 33.06 kcal/mol at CCSD(T)/6-31+G(d,p), which is reasonable agreement with the Ingold's estimation.

**S2** was reported to give exclusively *N*-alkoxyaminy radical adduct. As found in Table 7, the activation free energy of *N*-alkoxyaminy radical (8.83 kcal/mol) is much lower than that of aminoxyl radical (15.07 kcal/mol). As shown by the transition states depicted in Fig. 10, the nitroso nitrogen is likely to be protected by  ${}^t\text{Bu}$  groups. The steric hindrance by the *tert*-butyl groups determines the selectivity.

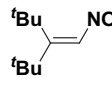
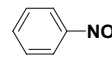
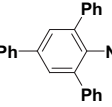
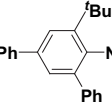
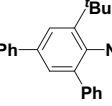
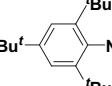
In the reaction of PhNO with  $\dot{\text{C}}\text{H}_3$  (**S3**), the activation free energy for the generation of PhMeNO is estimated to be 12.91 kcal/mol at CCSD(T)/6-31+G(d,p)//B3LYP/6-31+G(d,p), while that for the generation of PhNOME is much higher by 19.49 kcal/mol. Furthermore, the calculated heat of reaction shows that PhMeNO is thermodynamically more stable than PhNOME. When the steric congestion around the nitroso group is small, the radical attack at the nitroso nitrogen is predominant to yield aminoxyl radical.

Fig. 11 describes a Gibbs free-energy diagram for the reaction of 2,4-diphenyl-6-*tert*-butyl nitrosobenzene and 2-(methoxycarbonyl)-2-propyl radical (**S6**) at B3LYP/6-31+G(d,p). In the figure, TS3 and TS4 are transition states for N–C and O–C bond formations, respectively, and GS5 and GS6(**9**) are the corresponding products. The reported experimental ratio for GS6/GS5 was 3.7/1 in benzene at 80 °C<sup>13c</sup> and the theoretical activation free energies for TS3 and TS4 are 18.64 and 14.00 kcal/mol, respectively. The results



**Fig. 11.** The Gibbs free-energy diagram of reaction of 2,4-diphenyl-6-*tert*-butyl-nitrosobenzene and 2-(methoxycarbonyl)-2-propyl radical (**S6**). The numbers are relative free energies, and enthalpies in parentheses, based on **GS4** in kcal/mol estimated by B3LYP/6-31+G(d,p). The numbers around bonds indicate the bond distances in angstrom.

**Table 7**  
Calculated activation energies and heat of reactions of nitroso compounds,  $R^1NO$  and alkyl radicals,  $\dot{R}^2$

Run	$R^1NO$	$\dot{R}^2$	Exp.ratio of $R^1NOR^{2a}$	Product radical <sup>b</sup>	Ref	Activation energy (kcal/mol) <sup>c</sup>		Heat of reaction (kcal/mol) <sup>c</sup>	
						Gibbs E.	Enthalpy	Gibbs E.	Enthalpy
<b>S1</b>	<sup>t</sup> BuNO	$\dot{C}Me_3$		<b>31</b>	27	11.52	1.20	-16.01	-30.09
						(9.43) <sup>d</sup>	(-0.88)	(-23.63)	(-37.71)
<b>S2</b>		$\dot{C}Me_3$	1.00	$R^1\dot{N}OR^2$ $R^1R^2\dot{N}O$	35	12.72	1.40	-13.19	-28.69
						(9.25)	(-2.07)	(-21.25)	(-36.75)
						8.83	0.70	-24.12	-38.10
<b>S3</b>		$\dot{C}H_3$		PhNOMe PhMe $\dot{N}O$	13c	13.25	3.89	-26.99	-38.66
						(19.49)	(10.13)	(-23.26)	(-34.92)
						9.75	1.39	-35.38	-47.43
<b>S4</b>		$\dot{C}Me_2CO_2Me$	0.00	$R^1\dot{N}OR^2$ $R^1R^2\dot{N}O$	13c	13.41	2.99	-12.19	-24.31
						13.22	1.18	-9.95	-23.91
<b>S5</b>		$\dot{C}Me_2CN$	0.25	<b>4</b> $R^1R^2\dot{N}O$	12a	14.66	4.27	-9.75	-21.63
						17.31	5.58	-4.20	-17.51
<b>S6</b>		$\dot{C}Me_2CO_2Me$	0.79	<b>9</b> $R^1R^2\dot{N}O$	13c	14.00	3.89	-11.51	-23.06
						18.64	6.50	-3.34	-16.87
<b>S7</b>		$\dot{C}Me_2CN$	1.00	<b>14</b> $R^1R^2\dot{N}O$	28	17.93	6.90	-5.72	-17.66
						25.17	13.51	2.85	-10.75

<sup>a</sup> Experimental data, ratio is  $[R^1\dot{N}OR^2]/([R^1\dot{N}OR^2] + [R^1R^2\dot{N}O])$ , where the square bracket means a concentration.

<sup>b</sup>  $R^1R^2\dot{N}O$  and  $R^1\dot{N}OR^2$  denote an aminoxy and a *N*-alkoxyaminy radical.

<sup>c</sup> Gas-phase calculation at B3LYP/6-31+G(d,p) level.

<sup>d</sup> In parentheses, energies estimated at CCSD(T)/6-31+G(d,p)//B3LYP/6-31+G(d,p).

suggest that the generation of *N*-alkoxyaminy radical is predominant, which is in agreement with the experimental results. Fig. 12 plots the experimental ratio of two radical products against the difference in the theoretical activation energies for the four reactions, **S4–S7** (Table 7). The differences in the activation energies are calculated by subtracting the activation energy for O–C bond formations,  $E_a(\text{O–C})$ , from that for N–C bond formation,  $E_a(\text{N–C})$ , in the each reaction. When the difference is positively larger, the ratio of the O–C bond formation yielding *N*-alkoxyaminy radical becomes higher.

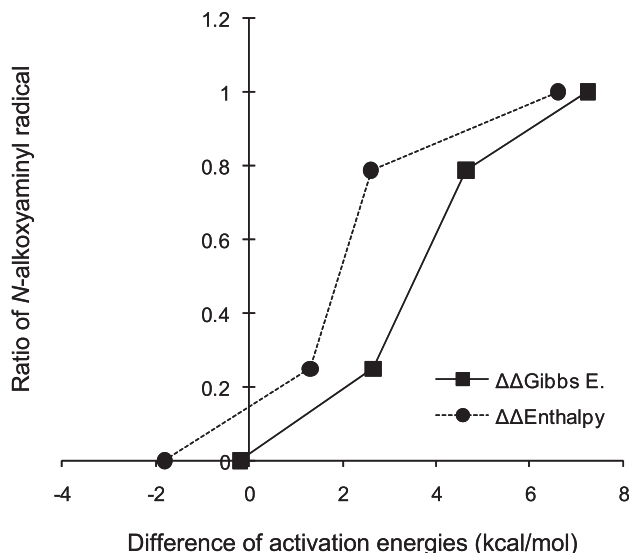


Fig. 12. Plot of differences of activation Gibbs free energies and enthalpies versus experimental ratios between *N*-alkoxyaminy and aminoxy radicals.

The correlation pattern is reasonable but the absolute theoretical energies are not satisfied with the experimental data. The differences in the activation free energies are too small to explain the experimental selectivity, if the Maxwell–Boltzmann distributions are calculated.

In **S3**, as the compared with CCSD(T), B3LYP underestimates  $E_a(\text{O–C})$  and  $E_a(\text{N–C})$  by 6.24 (=19.49–13.25) and 3.16 kcal/mol (=12.91–9.75), respectively, where the O–C and N–C bond formations yield PhNOMe and PhMeNO. We assumed that B3LYP erroneously underestimated the  $E_a(\text{O–C})$  for radical attack to nitrosobenzenes by 3.08 kcal/mol (=6.24–3.16) based on the  $E_a(\text{N–C})$ . Suppose the differences in the activation Gibbs free energies,  $\Delta\Delta G(=E_a(\text{N–C})-E_a(\text{O–C}))$ , in **S4** to **S7** at B3LYP/6-31+G(d,p) were adjusted by the subtraction of 3.08 kcal/mol (adj.  $\Delta\Delta G=E_a(\text{N–C})-(E_a(\text{O–C})+3.08)$ ), the estimated ratios based on the Maxwell–Boltzmann distribution at 80 °C would be significantly improved (Table 8).

Table 8

Predicted ratios of competing reactions from adjusted activation Gibbs free energies (in kcal/mol), and correlation data with experimental data

Run	Exp. ratio <sup>a</sup>	Calcd		Adj. calcd	
		$\Delta\Delta G^b$	Ratio <sup>a,c</sup>	$\Delta\Delta G^d$	Ratio <sup>a,c</sup>
<b>S4</b>	0.00	-0.19	0.44	-3.27	0.01
<b>S5</b>	0.25	2.65	0.97	-0.43	0.35
<b>S6</b>	0.79	4.64	1.00	1.56	0.90
<b>S7</b>	1.00	7.24	1.00	4.16	1.00
	$R^2$		0.584		0.983
	intercept		0.620		-0.047
	slope		0.455		0.983

<sup>a</sup>  $[\text{Ar}\dot{\text{N}}\text{OR}]/([\text{Ar}\dot{\text{N}}\text{OR}] + [\text{Ar}\dot{\text{R}}\text{NO}])$ .

<sup>b</sup> Gibbs free energy of  $E_a(\text{N–C})-E_a(\text{O–C})$  (kcal/mol).

<sup>c</sup> Maxwell–Boltzmann distribution calculated from  $\Delta\Delta G$  at 80 °C.

<sup>d</sup> Adj.  $\Delta\Delta G=\Delta\Delta G-3.08$  (kcal/mol).

Although the  $R^2$  between the experimental and the original theoretical ratios was only 0.584, the  $R^2$  of the adjusted theoretical ratios became 0.983. The errors of the DFT calculation (B3LYP/6-31+G(d,p)) would be improved by theoretical calculations at the higher accurate method, such as the coupled cluster approach.

#### 4. Conclusion

The studies confirmed that isotropic  $a_N$  and  $g$ -factors of *N*-alkoxyaminy radicals were reproduce with high accuracy at IEFFPCM/B3LYP/6-31+G(d,p). As for UV–vis spectra of *N*-alkoxyaminy radicals including aminoxy, IEFFPCM-TD-DFT could predict moderately experimental data and the functional PBE0 indicated better predictability than B3LYP, however the predicted wavelengths have been shifted to shorter than the experimental. The errors could be corrected by linear scaling approaches to precisely reproduce the UV–vis spectrum.

Generation of *N*-alkoxyaminy radical by reaction of nitroso compounds with alkyl radicals require steric congestions around nitroso groups and bulkiness of alkyl radicals. With the use of the DFT calculation, the trend of selectivity between two competing reactions was found to be predictable.

#### Supplementary data

Supplementary data related to this article can be found online at doi:10.1016/j.tet.2011.01.079. These data include MOL files and InChIKeys of the most important compounds described in this article.

#### References and notes

- (a) Hicks, R. G. *Org. Biomol. Chem.* **2007**, *5*, 1321; (b) Power, P. P. *Chem. Rev.* **2003**, *103*, 789.
- (a) Sheehan, D. *Physical Biochemistry*; John Wiley & Sons: UK, 2009; (b) Berliner, L. J. *Spin Labelling: Theory and Applications*; Academic: New York, NY, 1979; (c) Rehorek, D. *Chem. Soc. Rev.* **1991**, *20*, 341.
- (a) Morita, Y.; Kawai, J.; Fukui, K.; Nakazawa, S.; Sato, K.; Shiomi, D.; Takui, T.; Nakatsujii, K. *Org. Lett.* **2003**, *5*, 3289; (b) Zienkiewicz, J.; Kaszynski, P.; Young, V. C., Jr. *J. Org. Chem.* **2004**, *69*, 7525; (c) Lahti, P. M. *Magnetic Properties of Organic Materials*; Marcel Dekker: New York, Basel, 1999; (d) Uchida, Y.; Suzuki, K.; Tamura, R.; Ikuma, N.; Shimono, S.; Noda, Y.; Yamauchi, J. *J. Am. Chem. Soc.* **2010**, *132*, 9746.
- (a) Oyaizu, K.; Nishide, H. *Adv. Mater.* **2009**, *21*, 2339; (b) Barclay, T. M.; Cordes, A. W.; Haddon, R. C.; Itkis, M. E.; Oakley, R. T.; Reed, R. W.; Zhang, H. *J. Am. Chem. Soc.* **1999**, *121*, 969.
- (a) Adam, W.; Saha-Möllner, C. R.; Ganeshpure, P. A. *Chem. Rev.* **2001**, *101*, 3499; (b) Sheldon, R. A.; Arends, I. W. C. E. *Adv. Synth. Catal.* **2004**, *346*, 1051.
- Matyjaszewski, K.; Xia, J. *Chem. Rev.* **2001**, *101*, 2921.
- (a) McCarrroll, A. J.; Walton, J. C. *J. Chem. Soc., Perkin Trans. 2* **2000**, 2399; (b) Bella, A. F.; Slawin, A. M. Z.; Walton, J. C. *J. Org. Chem.* **2004**, *69*, 5926; (c) DiLabio, G. A.; Scanlan, E. M.; Walton, J. C. *Org. Lett.* **2005**, *7*, 155.
- Piloty, O.; Schwerin, B. G. *Chem. Ber.* **1901**, *34*, 1870.
- Balaban, A. T.; Frangopol, P. T.; Frangopol, M.; Negoia, N. *Tetrahedron* **1967**, *23*, 4661.
- Terabe, S.; Konaka, R. *J. Am. Chem. Soc.* **1971**, *93*, 4306.
- Danen, W. D.; West, C. T. *J. Am. Chem. Soc.* **1971**, *93*, 5582.
- (a) Miura, Y.; Tomimura, T. *Chem. Commun.* **2001**, 627; (b) Miura, Y.; Tomimura, T.; Matsuba, N.; Tanaka, R.; Nakatsujii, M.; Teki, Y. *J. Org. Chem.* **2001**, *66*, 7456.
- (a) Miura, Y.; Matsuba, N.; Tanaka, R.; Teki, Y.; Takui, T. *J. Org. Chem.* **2002**, *67*, 8764; (b) Miura, Y.; Nishi, T.; Teki, Y. *J. Org. Chem.* **2003**, *68*, 10158; (c) Miura, Y.; Muranaka, Y.; Teki, Y. *J. Org. Chem.* **2003**, *68*, 4786.
- Zakrassov, A.; Kaftory, M. *Cryst. Eng.* **2004**, *6*, 31.
- Hariharan, P. C.; Pople, J. A. *Theor. Chim. Acta* **1973**, *28*, 213.
- (a) Frisch, M. J.; Trucks, G. W.; Schlegel, H. B.; Scuseria, G. E.; Robb, M. A.; Cheeseman, J. R.; Montgomery, J. A., Jr.; Vreven, T.; Kudin, K. N.; Burant, J. C.; Millam, J. M.; Iyengar, S. S.; Tomasi, J.; Barone, V.; Mennucci, B.; Cossi, M.; Scalmani, G.; Rega, N.; Petersson, G. A.; Nakatsujii, H.; Hada, M.; Ehara, M.; Toyota, K.; Fukuda, R.; Hasegawa, J.; Ishida, M.; Nakajima, T.; Honda, Y.; Kitao, O.; Nakai, H.; Klene, M.; Li, X.; Knox, J. E.; Hratchian, H. P.; Cross, J. B.; Bakken, V.; Adamo, C.; Jaramillo, J.; Gomperts, R.; Stratmann, R. E.; Yazyev, O.; Austin, A. J.; Cammi, R.; Pomelli, C.; Ochterski, J. W.; Ayala, P. Y.; Morokuma, K.; Voth, G. A.; Salvador, P.; Dannenberg, J. J.; Zakrzewski, V. G.; Dapprich, S.; Daniels, A. D.; Strain, M. C.; Farkas, O.; Malick, D. K.; Rabuck, A. D.; Raghavachari, K.; Foresman, J. B.; Ortiz, J. V.; Cui, Q.; Baboul, A. G.; Clifford, S.; Cioslowski, J.; Stefanov,



- B. B.; Liu, G.; Liashenko, A.; Piskorz, P.; Komaromi, I.; Martin, R. L.; Fox, D. J.; Keith, T.; Al-Laham, M. A.; Peng, C. Y.; Nanayakkara, A.; Challacombe, M.; Gill, P. M. W.; Johnson, B.; Chen, W.; Wong, M. W.; Gonzalez, C.; Pople, J. A. *Gaussian 03, Revision D.02*; Gaussian: Wallingford CT, 2004; (b) Glendening, E. D.; Reed, A. E.; Carpenter, J. E.; Weinhold, F. *NBO Version 3.1*; 1995.
17. Becke, A. D. *J. Chem. Phys.* **1993**, *98*, 5648.
18. Becke, A. D. *J. Chem. Phys.* **1993**, *98*, 1372.
19. (a) Adamo, C.; Barone, V. *J. Chem. Phys.* **1999**, *110*, 6158; (b) Perdew, J. P.; Burke, K.; Ernzerhof, M. *Phys. Rev. Lett.* **1996**, *77*, 3865.
20. (a) Zaarycz, N.; Botek, E.; Champagne, B.; Sciannaméa, V.; Jérôme, C.; Detrembleur, C. *J. Phys. Chem. B* **2008**, *112*, 10432; (b) Villamena, F. A.; Liu, Y.; Zweier, J. L. *J. Phys. Chem. A* **2008**, *112*, 12607.
21. Casida, M. E.; Jamorski, C.; Casida, K. C.; Salahub, D. R. *J. Chem. Phys.* **1998**, *108*, 4439.
22. (a) Barone, V.; Bloino, J.; Biczysko, M. *Phys. Chem. Chem. Phys.* **2010**, *12*, 1092; (b) Champagne, B.; Guillaume, M.; Zutterman, F. *Chem. Phys. Lett.* **2006**, *425*, 105.
23. (a) Tomasi, J.; Mennucci, B.; Cancès, E. *Theochem* **1999**, *464*, 211; (b) Mennucci, B.; Tomasi, J.; Cammi, R.; Cheeseman, J. R.; Frisch, M. J.; Devlin, F. J.; Gabriel, S.; Stephens, P. J. *J. Phys. Chem. A* **2002**, *106*, 6102.
24. Pople, J. A.; Head-Gordon, M.; Raghavachari, K. *J. Chem. Phys.* **1987**, *87*, 5968.
25. (a) Kaupp, M.; Bühl, M.; Malkin, V. G. *Calculation of NMR and EPR Parameters*; Wiley-VCH: Weinheim, Germany, 2006; (b) Improta, R.; Barone, V. *Chem. Rev.* **2004**, *104*, 1231; (c) Engels, B.; Eriksson, L. A.; Lunell, S. *Adv. Quantum Chem.* **1996**, *27*, 297.
26. (a) Hermosilla, L.; Calle, P.; Vega, G.; Sieiro, C. *J. Phys. Chem. A* **2006**, *110*, 13600; (b) Barone, V.; Cimino, P.; Stendardo, E. *J. Chem. Theory Comput.* **2008**, *4*, 751; (c) Barone, V.; Cimino, P. *J. Chem. Theory Comput.* **2009**, *5*, 192; (d) Rogowska, A.; Kuhl, S.; Walcarious, A.; Champagne, B. *Phys. Chem. Chem. Phys.* **2007**, *9*, 828; (e) Yagi, T.; Kikuchi, O. *J. Phys. Chem. A* **1999**, *103*, 9132.
27. Woynar, H.; Ingold, K. U. *J. Am. Chem. Soc.* **1980**, *102*, 3813.
28. Terabe, S.; Konaka, R. *J. Chem. Soc., Perkin Trans. 2* **1973**, 369.
29. Ahrens, W.; Berndt, A. *Tetrahedron Lett.* **1973**, *14*, 4281.
30. Danen, W.; West, C. T.; Kensler, T. T. *J. Am. Chem. Soc.* **1973**, *95*, 5716.
31. Jacquemin, D.; Wathelet, V.; Adamo, C. *J. Chem. Theory Comput.* **2009**, *5*, 2420.
32. Nakahara, K.; Iwasa, S.; Iriyama, J.; Morioka, Y.; Suguro, M.; Satoh, M.; Cairns, E. *J. Electrochim. Acta* **2006**, *52*, 921.
33. (a) Cimino, P.; Pavone, M.; Barone, V. *Chem. Phys. Lett.* **2006**, *419*, 106; (b) Lalevé, J.; Allonas, X.; Jacques, P. *Theochem* **2006**, *767*, 143; (c) Gloria, A. A.; Tedeschi, A.; D'Errico, G.; Improta, R.; Franco, L.; Ruzzi, M.; Corvaia, C.; Barone, V. *J. Phys. Chem. A* **2002**, *106*, 10700.
34. Monat, J. E.; Rodriguez, J. H.; McCusker, J. K. *J. Phys. Chem. A* **2002**, *106*, 7399.
35. Ahrens, W.; Wieser, K.; Berndt, A. *Tetrahedron Lett.* **1973**, *14*, 3141.